Korean J. Chem. Eng., **31**(3), 436-445 (2014)
DOI: 10.1007/s11814-013-0260-z

pISSN: 0256-1115
eISSN: 1975-7220

Hydrodynamic behavior of inverse fluidized bed biofilm reactor for phenol biodegradation using *Pseudomonas fluorescens*

Sabarunisha Begum S.† and Radha K. V.

Department of Chemical Engineering, A C College of Technology, Anna University, Chennai - 600025, Tamil Nadu, India
(*Received 18 January 2013 • accepted 1 December 2013*)

Abstract−The hydrodynamic characteristic performance of an internal draft tube inverse fluidized bed biofilm reactor was studied for the aerobic biodegradation of phenol (1,200 mg/*l*) using *Pseudomonas fluorescens* for various ratios of settled bed volume to reactor working volume (V_b/V_r) under batchwise condition with respect to liquid phase. The operating parameters, such as superficial gas velocity, phase hold ups, aspect ratio and bed height, were analyzed for different ratios of (V_b/V_r). The effect of biodegradation on synthetic phenolic effluent was determined from the reduction in chemical oxygen demand and phenol removal efficiency. The optimum value of $(V_b/V_r)_m$ was 0.20 for the optimal superficial gas velocity, U_{gm}=0.220 m/s with the COD reduction efficiency of 98.5% in 48 hours. The biomass and biofilm characteristics of *P. fluorescens* were determined for optimal hydrodynamic operating parameters by evaluating its biofilm dry density and thickness, bioparticle density, suspended and attached biomass concentration.

Keywords: Fluidized Bed, Hydrodynamics, Hold Up, Phenol, Degradation

INTRODUCTION

Fluidized bed biofilm reactors (FBBR) that are conventionally used are mainly operated with upflow systems for either gas-solid, liquid-solid or gas-liquid-solid phases where the density of bioparticles (support particles coated with biofilm) is higher than the density of medium [1]. The achievement of high biomass concentration in FBBR makes for superior performance over that of the conventional packed bed fixed film bioreactor in a variety of waste water treatment applications. But the uncontrolled growth of biomass over support particles in FBBR leads to wash out of bioparticles from the reactor [2]. The biofilm thickness, which could not be controlled in FBBR, increases the mass transfer resistance and limits the diffusion of oxygen and/or organic substrate into the deeper layers of biofilm.

Inverse biofluidization is a relatively new technique where low density bioparticles are fluidized by either upward cocurrent flow of gas and liquid or by a downward flow of liquid and countercurrent upward flow of gas. In the former case, fluidization is achieved by upward flow of gas, making the bed to expand downwards, whereas in the latter case fluidization is done by the downward flow of liquid counter to the net buoyancy force of the particles. When the liquid flow is small and not sufficient to counter the net buoyancy force of the particles, inverse fluidization can also be achieved by upward flow of gas phase [3]. The application of low density support particles in an inverse fluidized bed biofilm reactor (IFBBR) overcomes the problem of normal upflow FBBR. The biofilm thickness can be easily maintained in IFBBR throughout the operation due to particle-particle collisions and particle-wall collisions inside the reactor [4]. This results in lesser mass transfer resistance, greater contact of solid-liquid-gas phases, large specific support surface area, fast biofilm formation and hence greater biodegradation effect [5]. IFBBR can separate the fluidized bed region from the gas-liquid contact region, which could reduce the shear due to bubble-particle collision on the biofilm [6,7]. Thus, a three phase inverse fluidized bed biofilm reactor can be successfully employed in all aerobic biotreatment of waste waters due to its high energy performance, low pressure drop, high gas holdup and high heat and mass transfer rates [8].

For the past decade considerable efforts have been made in exploring and understanding the hydrodynamic characteristics of fluid flow, heat and mass transfer effects in two and three phase fluidized bed systems. Fan et al. were the first to study the flow characteristics of inverse fluidization, utilizing low density spherical particles for both the liquid-solid and gas-liquid-solid systems [8]. They proposed correlations of the bed expansion and gas hold-up empirically and semi-empirically for the inverse gas-liquid-solid fluidization. Comte et al. studied the effect of hydrodynamic operating conditions (column diameter, gas sparger, initial weight of particles introduced into the reactor) of an inverse gas-liquid-solid turbulent bed and proposed a model to predict the values of specific gas velocities [9]. Krishna et al. studied the hydrodynamics of three phase inverse fluidized bed, which included pressure drop, minimum liquid and gas fluidization velocities and axial hold ups [10]. Sivasubramanian and Velan studied the influence of viscosity on minimum liquid and gas fluidization velocities and predicted correlations for minimum liquid fluidization velocity for Newtonian and non-Newtonian fluids [11]. Sokol studied the optimal operational range for a gas-liquid-solid inverse fluidized bed aerobic biofilm reactor with respect to settled bed volume to reactor volume, air velocity and residence time for the largest COD removals [2]. Ochieng et al. studied the hydrodynamic characteristics performance of a three phase fluidized bed bioreactor for brewery waste water and showed the influence of aspect ratio, phase hold up, superficial gas velocity on particle and liquid loadings [12]. Jena et al. characterized the hydrodynamic

†To whom correspondence should be addressed.
E-mail: sabarunisha@gmail.com

properties of gas-liquid-solid fluidized bed by keeping the gas velocity at a fixed value and by varying the liquid velocity, studying the effect of phase hold up, minimum liquid fluidization velocity, pressure drop for different particle size and static bed height [13]. Buffiere and Moletta investigated some hydrodynamic characteristics of inverse three-phase fluidized beds using two types of particles having different characteristics and observed two different expansion mechanisms: a pseudo-fluidized state and a fluidized state, both contributed to the solid mixing and axial solid distribution in the system [14]. Han et al. investigated effects of the superficial gas velocity and particle loading in gas-liquid-solid inverse fluidization air lift bioreactor and concluded that for any particle loading, the gas holdup in the riser increases with increasing superficial gas velocities [15]. Renganathan et al. studied the variation of average phase holdups with liquid velocity at constant gas velocity and observed that at constant gas velocity, the liquid holdup increases and solid holdup decreases with increasing liquid velocity due to the expansion of the bed under fluidized bed condition [16]. Gomez et al. immobilized derivatives of soybean peroxidase in a laboratory scale fluidized bed reactor to study their viability for use in phenol removal. The influence of the different operational variables on the process was also studied and a reactor model based on the experimental results that predicts the system's behavior both in steady and transient state was developed [17]. Choi and Shin studied the hydrodynamic characteristics of inverse fluidized bed having different driving forces, aeration and centrifugal force, for the application of waste water treatment in two different inverse fluidized bed reactors, and they identified that the inverse fluidized bed with aeration was more efficient than a reactor operated with centrifugal force [18]. Sowmeyan and Swaminathan evaluated the feasibility of an inverse fluidized bed reactor for the anaerobic digestion of distillery effluent with low density carrier materials; the system achieved 84% COD removal at an organic loading rate (OLR) of 35 kg COD/m^3/day [19].

The above survey of the literature revealed the work done on hydrodynamics on the three phase inverse fluidized bed reactor. However, most of the data available are concerned with hydrodynamic factors of the reactor and are limited in studying the biodegradation effects of the industrial effluent. It is therefore essential to study and correlate the optimal hydrodynamic operating parameters of the reactor with the biodegradation of hazardous toxic chemicals in industrial effluent for achieving more efficient biodegradation. The present study focuses mainly on gas phase fluidization in IFBBR by keeping the liquid velocity as a fixed value. It reveals the hydrodynamic aspects of IFBBR, such as flow regimes, aspect ratios, variation of gas, liquid and solid hold ups, for different superficial air velocity by varying the ratios of settled bed height volume to reactor volume for the aerobic biodegradation of synthetic phenol of higher concentration in inverse fluidized bed biofilm reactor with draft tube arrangement. The biomass and biofilm performance characteristics of the organism (*P. fluorescens*) were also studied for the optimal hydrodynamic operating parameters of the reactor.

MATERIALS AND METHODS

1. Experimental Setup and Reactor Design Configuration

The IFBBR is a tubular reactor constructed from Duran glass with height to diameter (H:D) ratio of 10 : 1. The overall height of the reactor was 105 cm and the diameter was 10 cm. The height of the inner draft tube was 70 cm and fixed at a height of 15 cm from the bottom of the reactor. The diameter of the draft tube was 5 cm. A mesh was placed at a height of 10 cm from the bottom of the draft tube to improve phase mixing. A converging-diverging conical insert was placed just above the draft tube to eliminate dead zones near the reactor wall and to avoid particle accumulation above the liquid level. The working volume of the reactor was 5.6 liters (Fig. 1). The ports were provided at the top and bottom of the reactor for liquid recirculation and air inlet respectively. Two spargers, one at the bottom (to prevent settling of particles) and the other at the side of the conical bottom (for fluidizing the bioparticles), were connected to their respective air pumps (Model HS1) and a valve to control the air flow rate. A peristaltic pump (Model RH-120S) was used for controlling the recycle liquid flow rate. Low density non-porous polystyrene beads having diameter of 3.5 mm, density of 863 kg/m^3, surface area to volume ratio of 1.714×10^3 m^{-1} were used as support particles. The reactor was operated in batch recirculation mode under non-sterile conditions.

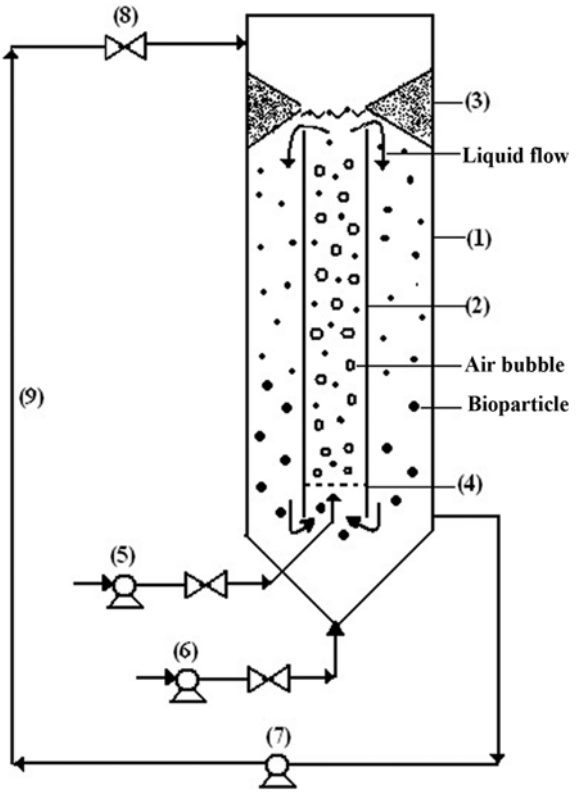

Fig. 1. Schematic representation of Inverse fluidized bed biofilm Reactor set up.

(1) IFBBR
(2) Draft tube
(3) Conical insert
(4) Mesh (3.8 mm jdia)
(5) Air pump (for fluidization)
(6) Sir pump (to prevent settling of bioparticles)
(7) Peristaltic pump
(8) Flow control valve
(9) Recycle stream

2. Bacterial Strain and Culture Medium

The microorganism *P. fluorescens* (MTCC No: 103) was chosen since it has the potential to degrade phenol and was used as the sole carbon and energy source. The preliminary stage of upstream processing work started with reviving the host by subsequent streaking of a mother culture of *P. fluorescens* on a Pseudomonas agar

slant (a differential media for fluorescein production) and keeping it for incubation at 28 °C for 2 days, until a definite quantum of pigment was produced in various subcultures [20,21]. The mineral salt medium has the following composition per liter: 700 ml deionized water, 100 ml buffer solution A, 100 ml trace elements solution B, 50 ml solution C and 50 ml solution D. Compositions of each solution were as follows: Buffer solution A composition: K_2HPO_4 - 1.0 g, KH_2PO_4 - 0.5 g, $(NH_4)_2SO_4$ - 0.5 g, deionized water 100 ml. Trace element solution B composition: NaCl - 0.5 g, $CaCl_2$ - 0.02 g, $MnSO_4$ - 0.02 g, $CuSO_4 \cdot 5H_2O$ - 0.02 g, H_3BO_3 - 0.01 g, deionized water - 50 ml. Solution C composition: $MgSO_4 \cdot 7H_2O$ - 0.5 g, deionized water - 50 ml, solution D composition: $FeSO_4$ - 0.02 g, Molybdenum powder - 0.02 g, deionized water - 50 ml. To prevent the precipitation of $CaSO_4$ and $MgSO_4$ in storage, the water, buffer solution A, trace elements solution B, solution C and solution D were autoclaved at 121 °C for 15 min [22]. After cooling, all the solutions were then mixed together and kept as stock solution from which known quantities were taken for the cultivation of the microorganisms. A primary culture was prepared by transferring two loops full of microorganisms from the agar slant into 100 ml of feed medium containing 20 ml of mineral salt medium and 80 ml of phenol from the initial substrate concentration of 1,200 mg/*l* in four 250 ml conical flasks. They were kept in a shaker incubator at 28 °C and agitated at 120 rpm until reaching a steady state of growth. The stationary phase was detected by analyzing the absorbance at 510 nm at regular time intervals. Once the microbe attained a steady state of growth, 10 ml of the primary culture was transferred into four 250 ml conical flasks, each containing 100 ml of the feed medium, and the incubation process was repeated. These were the secondary cultures used as inoculum for biofilm development over the support particle in IFBBR before the biodegradation process and this was done to adapt the microbe to that particular phenol concentration.

3. Experimental Procedure

Reactor was operated with 5.6 liters of feed medium having phenol concentration of 1,200 mg/*l*. Support particles were fed and secondary culture of *P. fluorescens* was incubated into the reactor for approximately 48 h to encourage cell growth and adhesion of freely suspended biomass on the particles. After the formation of biofilm onto support particles and attaining a well mixed and adapted culture, a fresh supply of the feed medium was fed with synthetic phenol effluent of concentration 1,200 mg/*l* with continuous supply of air for studying the hydrodynamic characteristics of IFBBR. The initial pH of the feed medium was 6.5 and the temperature was at 28 °C. During the biodegradation process, pH was slightly increased from 6.5 to 7.0 with the degradation of phenol, since it is a weak acid and tends to become slightly alkaline during its degradation. The pH of the feed medium was thus maintained and self-controlled within the optimal growth limit of the organism in the reactor [23]. Recycling was brought about with minimum flow rate of 40 ml/min, which increases the homogenization of the solution and prevents stagnant regions inside the reactor. The operation was carried out until there was complete removal of phenol in the reactor.

4. Measurement and Analysis

Samples were collected at regular intervals to estimate the phenol concentration, biomass concentration in suspended (suspension) and attached forms (biofilm), oxygen transfer rate (OTR) and volumetric mass transfer coefficient k_La, biofilm dry density, bioparticle density, biofilm thickness, chemical oxygen demand (COD) and pH. The reactor was allowed to run continuously till the analytical techniques showed that phenol was completely degraded. All determinations were performed according to standard procedures and methods [24].

Phenol concentration was measured by standard amino-pyrimetric method with absorbance measurements at 510 nm spectrophotometrically, while chemical oxygen demand (COD) was determined by standard methods of water analysis [25,26]. Suspended biomass concentration was determined by dry weight method, whereas the attached biomass concentration was measured by the increase of attached volatile solids on polystyrene support particles. The particles covered by biofilm (40-50 bioparticles) were taken from the top portion of the reactor, air dried at 110 °C for 2 hours, and their dry weight (the attached volatile solid) was found. The difference between the initial weight of support particles and the bioparticles was considered as the attached biomass weight and was expressed as (g_{AVS}/g_{solid}) [27,28]. The biofilm dry density and thickness of the biofilm were determined as calculated by Rabah and Dahab from the net dry biomass weight of the bioparticle [29].

Phase mixing was studied visually by observing the solid, liquid and gas phases [30]. Once the low density solid support particles were fed to the reactor having feed medium, they form a packed bed-like appearance at the top of the column. As the gas velocity is increased, first the bottom layer of the packed bed starts fluidizing. With further increase in gas velocity, the rest of the bed fluidizes and the bed begins to expand downwards first in the annular region and then it starts circulating throughout the reactor. At one particular gas velocity (minimum fluidization velocity), the entire bed is in fluidization condition, but the concentration of solid particles is not uniform throughout the bed inside the reactor. With further increase in gas velocity, there will be uniform concentration of solid particles throughout the reactor, and the velocity is termed as critical fluidization velocity [31,32]. Experiments were conducted to study the hydrodynamic characteristics of IFBBR by varying the ratio of volume of settled bed to working volume of the reactor (V_b/V_r), such as 0.10, 0.15, 0.20, 0.25 and 0.30, with different superficial air velocities, U_g which are just equal to or larger than the critical fluidization velocity, and the influence of phase hold up, aspect ratio, bed height and superficial air velocity was analyzed. Aspect ratio was altered by changing bed height at constant column diameter. The particle loading was such that the real volume of the particles was selected with respect to the ratio of settled bed height to reactor volume (V_b/V_r), which was in the range of 0.10, 0.15, 0.20, 0.25 and 0.30.

The following equations have typically been used to determine the volume fraction (holdup) of all phases and pressure drop per unit height ($\Delta P/H$) in the three phase inverse fluidized bed [13].

$$(\Delta P/H)=(\varepsilon_s\rho_s+\varepsilon_l\rho_l+\varepsilon_g\rho_g)g \quad (1)$$

$$(\varepsilon_g+\varepsilon_s+\varepsilon_l)=1 \quad (2)$$

$$\varepsilon_s=M_s/(H_sA\rho_s) \quad (3)$$

where ε_g, ε_s, ε_l are gas, liquid and solid holdups, respectively; ρ_g, ρ_s and ρ_l similarly represent densities; g is acceleration due to gravity. From Eq. (1) it is evident that high density particles lead to high pressure drop, causing increase in power consumption. Thus, the application of low density particles in IFBBR with draft tube arrange-

ment can minimize this tendency [12].

The average phase holdups are measured by the following relation:

$$\varepsilon_s=(V_s/V_r) \quad (4)$$

$$\varepsilon_g=(Z_f-Z_i)/Z_f \quad (5)$$

where V_s, V_r are volume of solid particles and working volume of the reactor respectively; Z_f, Z_i are the aerated liquid level in the reactor column after fluidization and the initial liquid level before aeration, respectively.

RESULTS AND DISCUSSION

The hydrodynamic behavior of IFBBR has been studied for the biodegradation of synthetic effluent containing 1,200 mg/*l* of phenol by varying the ratio of settled bed height to reactor volume (V_b/V_r) in the range of 0.10, 0.15, 0.20 and 0.25 for various superficial air velocities U_g for each (V_b/V_r) ratio. To optimize the ratio (V_b/V_r) and superficial air velocity U_g with greater accuracy, experiments were performed for various ratios of (V_b/V_r) with three different superficial gas velocities U_g: (i) V_b/V_r=0.10, U_g=0.089 m/s, 0.095 m/s and 0.099 m/s (ii) V_b/V_r=0.15, U_g=0.152 m/s, 0.157 m/s and 0.165 m/s (iii) V_b/V_r=0.20, U_g=0.216 m/s, 0.220 m/s and 0.224 m/s (iv) V_b/V_r=0.25, U_g=0.274 m/s, 0.278 m/s and 0.281 m/s) and all the experimental analyses were done in triplicate. The influence of operating parameters, such as phase hold up, aspect ratio, settled bed height and superficial air velocity, was analyzed. The particle loading was varied to determine the effect of phase holdup on bed homogeneity. The ranges in which particle loading and bed height affect fluidization, and consequently chemical oxygen demand (COD) reduction, were determined.

1. Optimization of Superficial Air Velocity, U_{gm}

Experiments were performed for various ratios of (V_b/V_r) with different superficial air velocities, U_g to optimize U_g for each (V_b/V_r) ratio. To identify the optimal superficial velocity U_{gm}, the optimization function adopted was the largest COD reduction and phenol removal efficiency. Note that the superficial air velocities, U_g, applied on the experiments were equal to and just larger than the critical fluidization velocity, U_{gcr}, below which the fluidization of particles was not uniform throughout the reactor [32]. Experiments were repeated for first four sets of values of V_b/V_r such as 0.10, 0.15, 0.20 and 0.25 with its respective superficial air velocities, U_g, and were not carried out for the last set of ratio (V_b/V_r)=0.30, which was found to be the critical (V_b/V_r) ratio at and above which the fluidization of

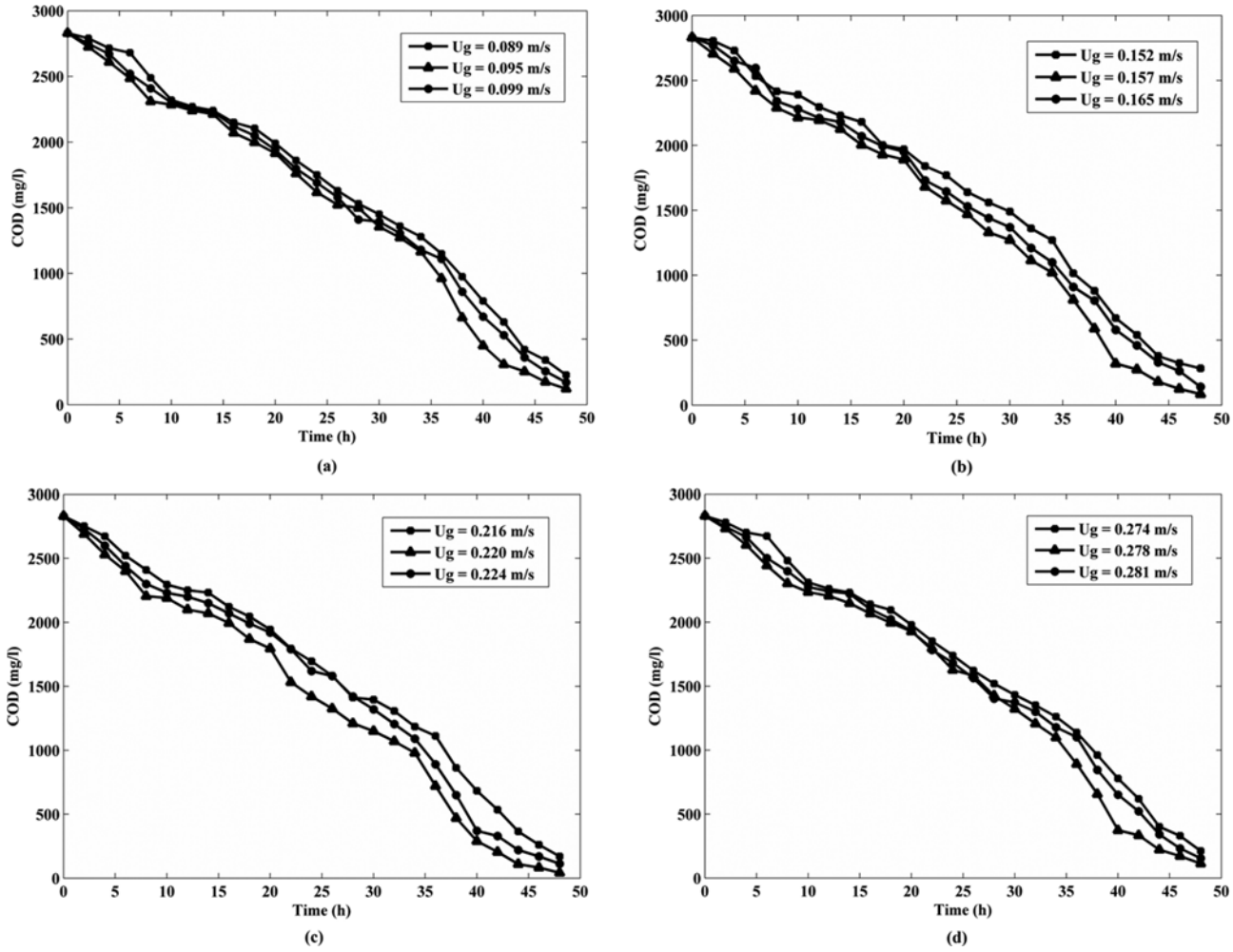

Fig. 2. Variation of COD values with time for various ratios of (V_b/V_r) and superficial air velocities, U_g.
(a) (V_b/V_r)=0.10, (b) (V_b/V_r)=0.15, (c) (V_b/V_r)=0.20, (d) (V_b/V_r)=0.25

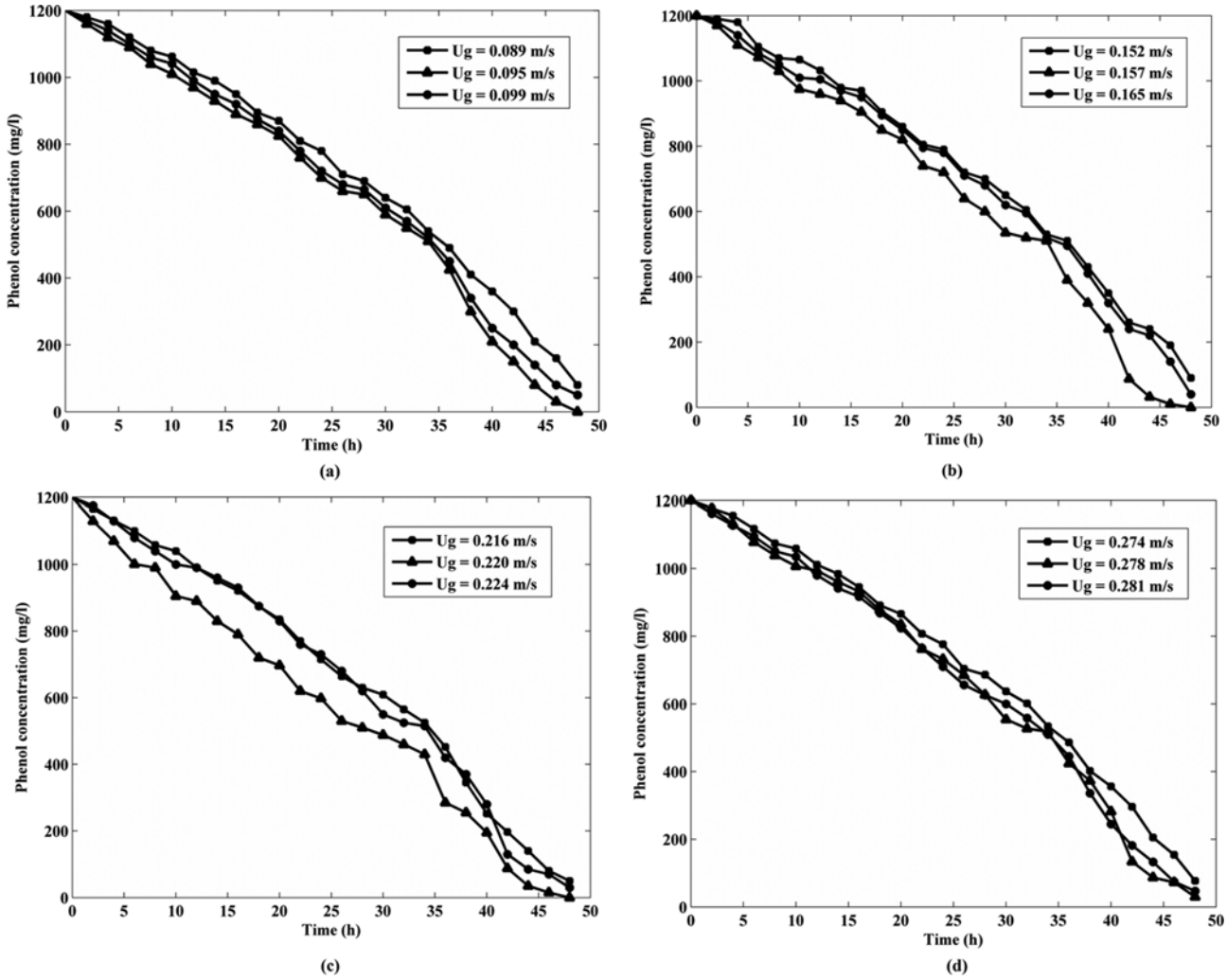

Fig. 3. Variation of phenol concentration with time for various ratios of (V_b/V_r) and superficial air velocities, U_g.
(a) (V_b/V_r)=0.10, (b) (V_b/V_r)=0.15, (c) (V_b/V_r)=0.20, (d) (V_b/V_r)=0.25

the solid particles was impossible; the particles settled as a packed bed at the top of the reactor once the fluidization was started [12].

Figs. 2 and 3 show that the decrease in COD and phenol concentration values depended on the ratio (V_b/V_r) and superficial air velocity U_g. The largest COD and phenol reduction was attained at an optimum superficial air velocity, U_{gm} for each (V_b/V_r) ratio. Optimal superficial air velocities, U_{gm} for different ratio of (V_b/V_r) with respect to phenol and COD reduction are shown in Table 1.

This can be explained by the fact that for a particular value of superficial air velocity (optimal superficial air velocity, U_{gm}) there will be higher COD reduction in the biodegradation process due to higher gas holdup ε_g, volumetric mass transfer coefficient k_La and oxygen transfer rate (OTR) [33,34]. Table 2 shows the effect of superficial air velocity on mean values of volumetric mass transfer coefficient k_La, OTR and biofilm characteristics for the optimized settled bed height to reactor volume [$(V_b/V_r)_m$=0.20] where the largest COD removal of 98.5% and phenol degradation of 100% was attained (Table 1).

From Table 2, k_La and OTR increased with increase in superficial air velocity, U_g due to increase of gas holdup ε_g and gas-liquid interfacial area, a. In all the three phase fluidized bed biofilm reactors, gas phase holdup ε_g and bubble size d_b increased with increasing U_g, and if the gas-liquid interfacial area has a relation of $a=6\varepsilon_g/$

Table 1. Optimal superficial air velocities, U_{gm} for different ratio of settled volume to working volume, V_b/V_r

Sl. No.	(V_b/V_r)	U_g (m/s)	COD reduction (%)	Phenol removal efficiency (%)
1	0.10	0.089	92.0	93.3
		0.095 (U_{gm})	**95.7**	**100.0**
		0.099	94.0	95.8
2	0.15	0.152	90.0	92.5
		0.157 (U_{gm})	**97.0**	**100.0**
		0.165	95.0	96.7
3	0.20	0.216	94.0	95.8
	$(V_b/V_r)_m$	**0.220 (U_{gm})**	**98.5**	**100.0**
		0.224	96.0	97.5
4	0.25	0.274	92.5	93.6
		0.278 (U_{gm})	**96.0**	**97.5**
		0.281	94.5	96.9

Table 2. Effect of superficial air velocity on k_La, OTR and biofilm charaterictics for the $(V_b/V_r)_m$=0.20

Parameters	Superficial air velocity, U_g in m/s		
	U_{g1}	$U_{g2}=U_{gm}$	U_{g3}
	0.216	0.220	0.224
Mean oxygen transfer rate, $(OTR)_{avg}$, in g/(l·min)	0.0113	0.0159	0.0136
Mean volumetric mass transfer coefficient, $(k_La)_{avg}$ in min^{-1}	1.3376	1.8823	1.6119
Gas hold up, ε_g	0.0642	0.0653	0.0660
Mean biofilm thickness, $(L_f)_{avg}$ in μm	158	137	149
Mean biofilm dry density, $(X_f)_{avg}$, kg/m^3	76.3	83.8	80.1
Average attached biomass conc., in $(g_{AVS}/g_s)_{avg}$	0.0185	0.0294	0.0198
Average bioparticle density, $(\rho_b)_{avg}$, kg/m^3	891	885	889

d_b, the increase in ε_g produces higher a, but the increase of bubble size d_b decreases a. When the increased rate of ε_g dominates over that of d_b, the k_La increases with increasing U_g. Because of these two competing effects, the increasing trend of k_La becomes insignificant with increasing U_g [35]. Thus, at higher air velocity above optimal, the bubble size dominates over the interfacial area, resulting in lesser mass transfer rate, and the degree of turbulence distribution becomes poorer owing to the irregular distribution of big size bubbles in the bed, affecting the biodegradation effects of phenol [36,37].

Moreover, an increase in superficial gas velocity produces higher detachment force on the biofilm, which decreases biofilm thickness until it reaches the optimum superficial velocity, which produces compact and stable biofilm structure. Above U_{gm}, the thickness of the biofilm increases where the detachment force does not control the outgrowth of biofilm anymore [38] and the growth of the biofilm is found to be higher than the detachment from the surface. The higher detachment force removes fluffy and less dense newly grown biomass on the outer layers of the particles [39].

The biofilm dry density is a function of biofilm thickness. Bioparticles with lesser biofilm thickness produce more stable and highly dense biofilm due extra biomass growth (in the form of micro colonies) in the base biofilm, whereas the bioparticles with thicker biofilm have lower biofilm dry density [40]. Thus, the average biofilm dry density, $(X_f)_{avg.}$, was found to be increasing with superficial velocity; U_g then again decreased.

Attached biomass was measured from the dry mass of attached volatile solids per dry mass of the support particle, $(g_{AVS}/g_s)_{avg.}$ Increase in superficial velocity produces thinner biofilms which are more stable, dense and have higher dry density of the biofilm, resulting in more dry mass of attached volatile solids. Thus, the attached biomass concentration increases with superficial velocity till the optimum and then decreases.

2. Optimization of Settled Bed Height Volume to Reactor Volume, $(V_b/V_r)_m$

Biodegradation effects of phenol were studied for various ratios of (V_b/V_r) at the optimized superficial air velocity, U_{gm} (Figs. 2 and 3, Table 1).

With an increase in settled bed height volume of particles, the optimal superficial velocity also increased due to more air needed by large amount of bioparticles for biomass growth. From Figs. 2(c), 3(c) and Table 1, the largest COD removal of 98.5% and phenol degradation of 100% was attained when (V_b/V_r)=0.20 at its optimal superficial velocity, U_{gm}=0.220 m/s. An increase in COD removal with an increase in (V_b/V_r) from 0.10 to 0.20 can be attributed to the fact that for the increasing (V_b/V_r) there will be more biomass grown on large volume of particles, resulting in higher degradation of phenol. But with further increase in (V_b/V_r) from 0.2 to 0.3, a larger volume of the reactor was occupied by support particles, leading to higher solid holdup which worsened the phase mixing characteristics of the reactor and resulted in a decrease in biodegradation effect [41,42]. The ratio (V_b/V_r)=0.3 was found to be the critical value at and above which the fluidization of particles was impossible as it settled at the top of the reactor. Hence, $(V_b/V_r)_m$=0.20, U_{gm}= 0.220 m/s at 48 h of bioreactor operation were found to be the optimal hydrodynamic values at which the COD was decreased from an original value of 2,830 to 42 mg/l with 98.5% removal efficiency.

3. Effect of Settled Bed Height on Optimal Superficial Gas Velocity

The effect of (V_b/V_r) on U_{gm} and its biodegradation outcomes are depicted in Figs. 4 and 5. As (V_b/V_r) ratio increased, U_{gm} also increased (Fig. 4). This is because as the number of particles increased, the gas velocity required to fluidize the bed was naturally high and hence the superficial air velocity increased [2].

With increase in ratio of (V_b/V_r), there was an initial increase in biodegradation until (V_b/V_r)=0.20 and then decreases (Fig. 5). This increase might be due to the availability of more surface area for

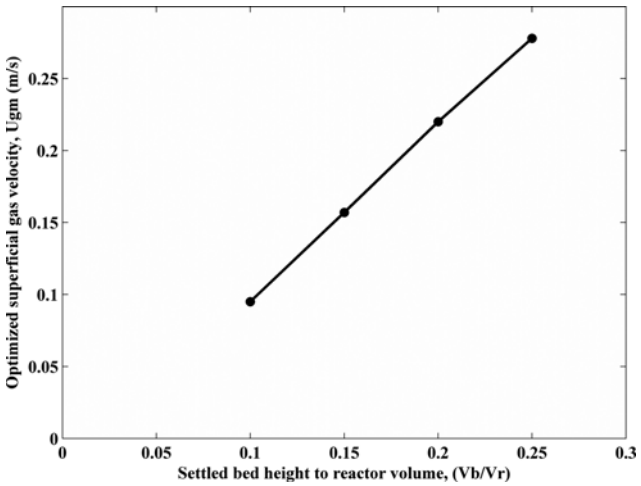

Fig. 4. Variation of optimized superficial gas velocity, U_{gm} with settled bed height to reactor volume, (V_b/V_r).

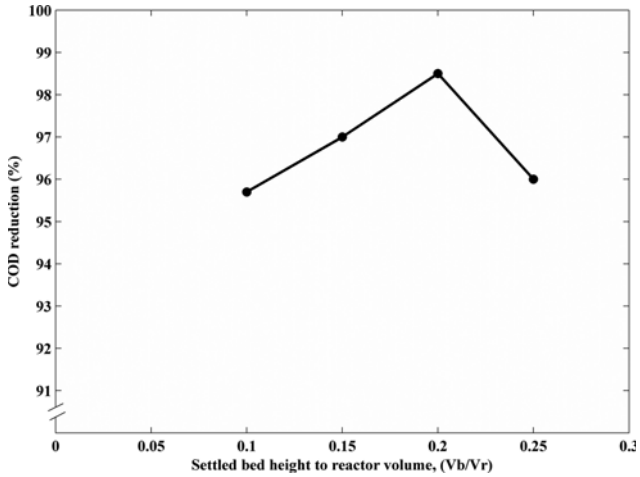

Fig. 5. Variation of COD reduction (%) with (V_b/V_r) for the optimized superficial gas velocity, U_{gm}.

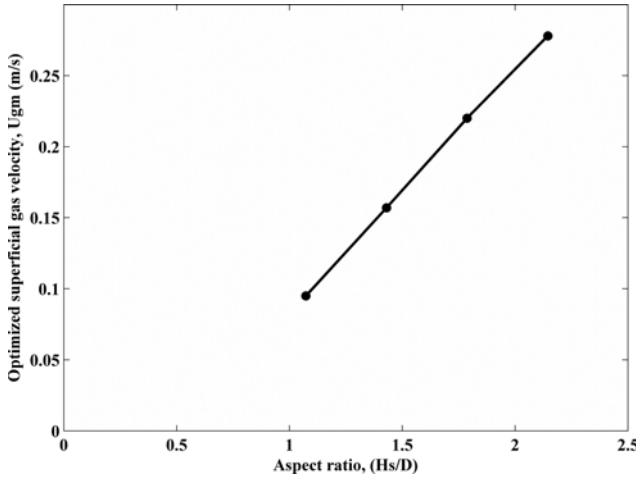

Fig. 6. Variation of aspect ratio, H_s/D with optimized superficial gas velocity, U_{gm} (m/s).

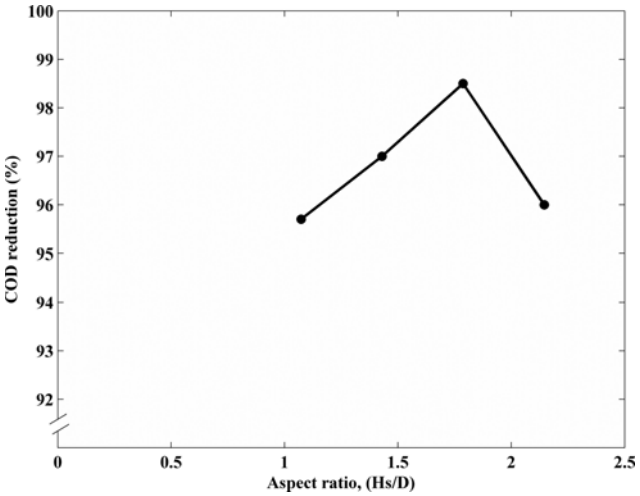

Fig. 7. Variation of COD reduction (%) with aspect ratio, H_s/D for the optimized superficial gas velocity, U_{gm}.

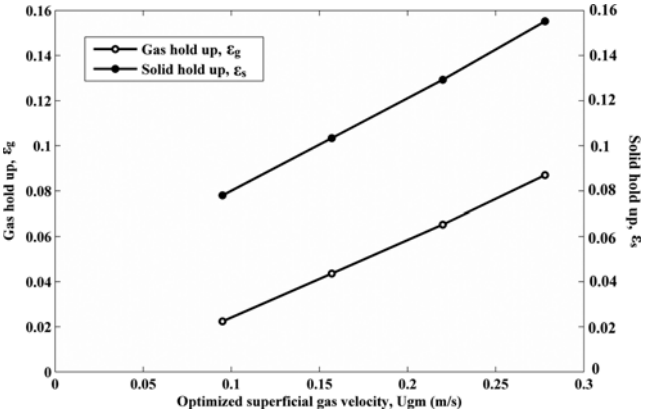

Fig. 8. Variations of solid hold up, ε_s and gas hold up, ε_g with optimized superficial gas velocity, U_{gm}.

microbial attachment onto large number of support particles. But with further increase in particle loading, the solid holdup greatly increased, resulting in improper and poor phase mixing characteristics and the fluidization led to decrease the biodegradation effect.

4. Effect of Aspect Ratio on Superficial Gas Velocity and COD Reduction

Fig. 6 illustrates the effect of aspect ratio (height of the settled bed, H_s/column diameter, D) of the reactor with optimal superficial gas velocity, U_{gm}. The aspect ratio increased when the height of the settled bed increased. With increase in particle loading, the particles needed high velocity to fluidize uniformly throughout the reactor, which in turn increased its superficial gas velocity, U_{gm}. Also as the particle loading increased, larger number of particles needed more oxygen for growth and metabolism.

As depicted in Fig. 7, COD removal efficiency increased till a particle aspect ratio, H_s/D, of 1.787. Beyond that it decreased as the over loading of particles worsened the phase mixing and fluidization characteristics of the reactor, leading to cell lysis due to oxygen deficiency [12].

5. Effect of Optimal Superficial Gas Velocity and Gas Holdup on COD Removal

Fig. 8 shows the variation of gas and solid holdups with optimal superficial gas velocity, U_{gm} obtained for different (V_b/V_r) ratios and shows a linear relation between them. As the superficial gas velocity increased the volume fraction occupied by the gas also increased, leading to increased gas holdup in the reactor [43]. Due to higher particle loading at each (V_b/V_r) ratio corresponding to its optimal superficial gas velocities, volume fraction of solid increased, leading to increased solid holdup.

Fig. 9 shows the effect of optimal superficial air velocity and phase holdup (obtained for the ratio of (V_b/V_r)=0.10, 0.15, 0.20 and 0.25) on biodegradation of phenol. The optimal superficial air velocity for maximum COD reduction of 98.5% was 0.220 m/s with a corresponding gas holdup of 0.0653. Further increase in gas holdup and superficial gas velocity decreased the biodegradation efficiency of phenol due to poor phase mixing characteristics caused by higher particle loading inside the reactor [44].

6. Pressure Drop (ΔP/H) and Superficial Gas Velocity in Three Phase IFBBR

Variations of pressure drop per unit height of column with super-

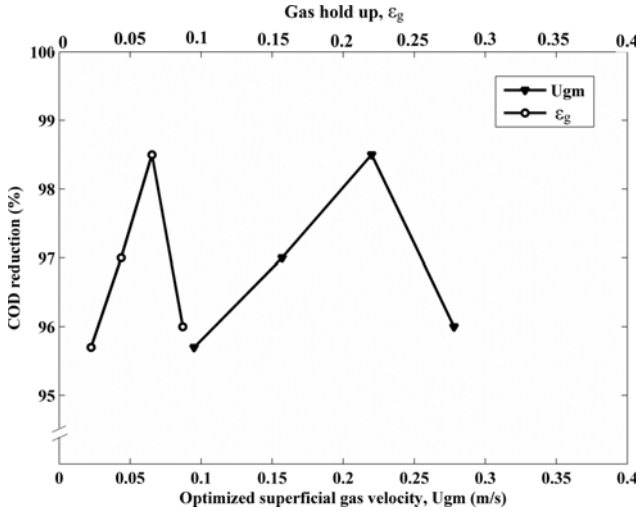

Fig. 9. Effect of optimal superficial gas velocity, U_{gm} and gas hold up, ε_g on biodegradation of phenol.

Table 3. Pressure drop ($\Delta P/H$) and superficial gas velocity, U_g for different ratios of V_b/V_r

(V_b/V_r)	U_g, m/s	$(\Delta P/H)$, N/m^3
0.10	0.089	10134.75
	0.095	10121.09
	0.099	10108.49
0.15	0.152	9858.93
	0.157	9846.32
	0.165	9820.06
0.20	0.216	9576.83
	0.220	9565.27
	0.224	9557.92
0.25	0.274	9295.77
	0.278	9284.22
	0.281	9276.66

ficial gas velocity, U_g, for different ratios of (V_b/V_r) in IFBBR are tabulated in Table 3. From the experimental results it was observed that pressure increased with velocity and height of column until it reached a minimum fluidization velocity, after which the bed expanded at constant level and became completely fluidized, leading to constant values of pressure drop [11].

7. Biomass and Biofilm Characteristics of *P. fluorescens* in IFBBR at its Optimized Hydrodynamic Operating Values

Figs. 10 and 11 show the biomass characteristics and biofilm performance of *P. fluorescens* including biofilm dry density and thickness, bioparticle density, suspended and attached biomass concentration evaluated at optimized hydrodynamic operating parameters ($(V_b/V_r)_m$=0.20; U_{gm}=0.220 m/s; t=48 h) of IFBBR.

It can be seen from Fig. 10 that during the biodegradation process, the suspended biomass concentration increased for a short period of time due to the attrition of biofilm into bulk liquid. It was then followed by a steady decrease in its concentration due to the inhibition effect of substrate and that might also be due to the reattachment of biomass onto support particles [45]. Even with the decrease in suspended biomass concentration over the period of the biodegradation process, the COD values decreased proportionally with decreasing phenol concentration (Figs. 2 and 3) in the reactor, which could only be due to the well adapted, constant thickness maintained (Fig. 11) and highly tolerated biofilm culture to higher concentration of phenol. As the diameter of the bioparticles increased due to the formation of biofilm on the surface of particle, the bioparticle density increased. The average bioparticle density and biofilm dry density were found to be 885.48 kg/m^3 and 83.8 kg/m^3.

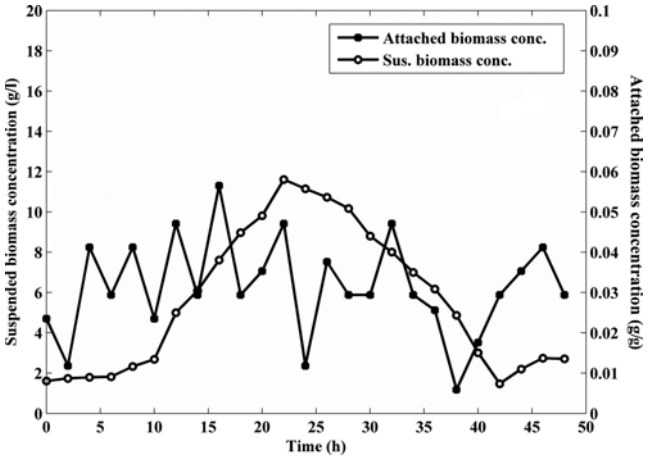

Fig. 10. Biomass characteristics of *P. fluorescens* in IFBBR at its optimized hydrodynamic operating conditions ($(V_b/V_r)_m$= 0.20; U_{gm}=0.220 m/s; t=48 h).

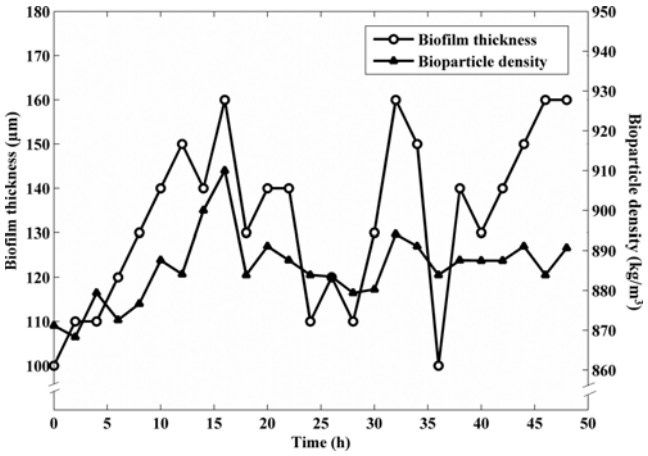

Fig. 11. Biofilm performance of *P. fluorescens* in IFBBR at its optimized hydrodynamic operating conditions ($(V_b/V_r)_m$=0.20; U_{gm}=0.220 m/s; t=48 h).

The attached biomass concentration increased with biofilm thickness. At the end of the biodegradation process, the attached biomass concentration (g_{AVS}/g_{solid}) was 0.0294 (g_{AVS}/g_{solid}). The thickness of the biofilm was almost maintained constant (120-160 μm) (Fig. 11) throughout the process due to the provision of mesh at the lower end of draft tube opening in IFBBR where some of the biofilm is removed by attrition; and might also be due to particle-particle attrition and particle-wall collision inside the reactor. The mean biofilm thickness was 137 μm. This effective control of biofilm thickness in IFBBR resulted in lesser mass transfer resistance, greater contact of solid-liquid-gas phases and hence greater phenol and COD removal

efficiency. Table 2 shows the effect of superficial air velocity on biofilm characteristics for the optimized hydrodynamic conditions.

CONCLUSIONS

Hydrodynamic characteristic performance of a three phase inverse fluidized bed biofilm reactor was studied experimentally for the application of phenol biodegradation. Experiments were carried out for various ratios of (V_b/V_r) at different superficial air velocities. COD removal increased with increase in U_g and (V_b/V_r), attaining higher removal efficiency at U_{gm} and $(V_b/V_r)_m$ and decreased with further increase in U_g and (V_b/V_r). The largest COD removal from 2,830 to 42 mg/*l* (98.5% COD reduction) was achieved when the reactor was operated at the ratio $(V_b/V_r)_m$=0.20 with superficial air velocity, U_{gm}=0.220 m/s in 48 h, showing the optimal operating parameters for IFBBR. Gas holdup increased with U_g whereas the biodegradation began decreasing after it reached U_{gm} of 0.220 m/s and ε_g of 0.0653. Particle loading affected the aspect ratio of the reactor. Biodegradation started decreasing when the aspect value was greater than 1.787, above which the volume fraction of solid particles affected the phase mixing inside the reactor leading to decrease in mass transfer effect. Biofilm performance and biomass characteristics of *P. fluorescens* were also evaluated at the optimal operating conditions of IFBBR.

NOMENCLATURE

A : cross sectional area of the column [m^2]
a : gas-liquid interfacial area [m^2/m^3]
COD : chemical oxygen demand [mg/*l*]
D : column diameter [m]
d_b : bubble size [m]
H : height of column [m]
H_s : height of settled bed [m]
k_La : volumetric mass transfer coefficient [min^{-1}]
L_f : biofilm thickness [μm]
M_s : mass of solid particles [kg]
OTR : oxygen transfer rate [g/(*l*·min)]
ΔP : pressure drop [N/m^2]
t : operation time [h]
U_g : superficial air (gas) velocity [m/s]
U_{gcr} : critical fluidization velocity [m/s]
U_{gm} : optimized superficial gas velocity [m/s]
V_b : volume of settled bed height [m^3]
V_r : volume of reactor (working volume) [m^3]
X_f : biofilm dry density [kg/m^3]
Z_f : aerated liquid level in column after fluidization [m]
Z_i : initial liquid level in column before aeration [m]
ε_g : gas hold up
ε_s : solid hold up
ε_l : liquid hold up
ρ_b : bioparticle density [kg/m^3]
ρ_g : density of gas phase [kg/m^3]
ρ_s : density of solid phase [kg/m^3]
ρ_l : density of liquid phase [kg/m^3]
g : acceleration due to gravity [m/s^2]
g_{AVS} : mass of bioparticle (in terms of attached volatile solid) [g]
g_{solid} : mass of solid support particle [g]

REFERENCES

1. L. S. Fan, *Gas-liquid-solid fluidization engineering*, Butterworths, Boston, USA (1989).
2. W. Sokol, *Int. J. Chem. React. Eng.*, **8**, 1 (2010).
3. W. Sokol and M. R. Hanafi, *Biochem. Eng. J.*, **3**, 185 (1999).
4. L. Nikolov and D. Karamenew, *Can. J. Chem. Eng.*, **65**, 214 (1987).
5. N. Ulaganathan and K. Krishnaiah, *Bioproc. Biosyst. Eng.*, **15**, 159 (1996).
6. A. Garnier, C. Chavarie, G. Andre and D. Klvana, *Chem. Eng. Commun.*, **98**, 31 (1990).
7. G. Olivieri, A. Marzocchella and P. Salatino, *Can. J. Chem. Eng.*, **88**, 574 (2010).
8. L. S. Fan, K. Muroyama and S. H. Chern, *Chem. Eng. J.*, **24**, 143 (1982).
9. M. . Comte, D. Bastoul, G. Hebrard, M. Roustan and V. Lazarova, *Chem. Eng. Sci.*, **52**, 3971 (1997).
10. S. V. Krishna, S. R. Bandaru, D. V. S. Murthy and K. Krishnaiah, *China Part.*, **5**, 351 (2007).
11. V. Sivasubramanian and M. Velan, *J. Chem. Eng. Japan*, **37**, 1436 (2004).
12. A. Ochieng, T. Ogada, W. Sisenda and P. Wambua, *J. Hazard. Mater.*, **90**, 311 (2002).
13. H. M. Jena, B. K. Sahoo, G. K. Roy and B. C. Meikap, *Chem. Eng. J.*, **145**, 50 (2008).
14. P. Buffiere and R. Moletta, *Chem. Eng. Sci.*, **54**, 1233 (1999).
15. S. J. Han, R. B. H. Tan and K. C. Loh, *Trans IChemE*, **78**, (2000).
16. T. Renganathan and K. Krishnaiah, *Chem. Eng. Sci*., **60**, 2545 (2005).
17. L. Gomez, A. Bodalo and E. Gomez, *Chem. Eng. J.*, **127**, 47 (2006).
18. H. S. Choi and M.-S. Shin, *Korean J. Chem. Eng.*, **16**(5), 670 (1999).
19. R. Sowmeyan and C. Swaminathan, *Bioresour. Technol.*, **99**, 3877 (2008).
20. A. A. U. de Souza, H. L. Brandao, I. M. Zamporlini, H. M. Soares and S. M. de A. G. U. de Souza, *Res. Conserv. Recycl.*, **52**, 511 (2008).
21. R. Souza, I. T. L. Bresolin, T. L. Bioni, M. L. Gimenes and B. P. Dias, *Braz. J. Chem. Eng.*, **21**, 219 (2004).
22. S. E. Agarry and B. O. Solomon, *Int. J. Environ. Sci. Technol*., **5**, 223 (2008).
23. D. Kotresha and G. M. Vidyasagar, *Biotechnol. Bioeng.*, **33**, 987 (2007).
24. APHA-AWA-WPCF1992, *Standards methods for the examination of water and waste water*, Sixteenth Ed., American Public Health Association, American Water Works Association: Water Pollution Control Federation, Washington, DC, USA (1992).
25. R. D. Yang and A. E. Humphrey, *Biotechnol. Bioeng.*, **17**, 1211 (1975).
26. S. E. Agarry and B. O. Solomon, *Int. J. Environ. Sci. Technol.*, **5**, 223 (2008).
27. M. Rajasimman and C. Karthikeyan, *Front. Chem. Eng. China*, **3**, 235 (2009).
28. K. J. F. Rabah and F. M. Dahab, *Water Res.*, **38**, 4262 (2004).
29. L. S. Fan, S. J. Hwang and A. Matsuura, *Chem. Eng. Sci.*, **39**, 1677 (1984).
30. T. Renganathan and K. Krishnaiyah, *Can. J. Chem. Eng.*, **81**, 853

(2003).
31. W. Sokol, A. Ambaw and B. Woldeyes, *Chem. Eng. J.*, **150**, 63 (2009).
32. J. C. Lee and P. S. Buckley, *Fluid mechanics and aeration characteristics of fluidized beds*, In: P. F. Cooper, B. Atkinson (Ed.), *Biological fluidized bed treatment of water and wastewater*, Ellis Horwood, Chichester, UK (1981).
33. W. T. Tang and L. S. Fan, *AIChE J.*, **33**, 239 (1987).
34. G. Olivieri, M. E. Russo, A. Marzocchella and P. Salatino, *Biotechnol. Prog.*, **27**, 1599 (2011).
35. S. D. Kim and Y. Kang, *Chem. Eng. Sci.*, **52**, 3639 (1997).
36. N. Arun, A. A. Razack and V. Sivasubramanian, *Chem. Eng. Commun.*, **200**, 1260 (2013).
37. I. Coelhoso, R. Boatventura and A. Rodriguez, *Biotechnol. Bioeng.*, **40**, 625 (1992).
38. Y. Liu and J.-H. Tay, *Water Res.*, **36**, 1653 (2002).
39. H. Beyenal and A. Tanyolac, *Biochem. Eng. J.*, **1**, 53 (1998).
40. W. K. Kwok, C. Picioreanu, S. L. Ong, M. C. M. van Loosdrecht, W. J. Ng and J. J. Heijnen, *Biotechnol. Bioeng.*, **58**, 400 (1998).
41. K. Fujie, H. Y. Hu, Y. Ikeda and K. Urano, *Chem. Eng. Sci.*, **47**, 3745 (1992).
42. R. C. Chen, J. Reese and L. S. Fan, *AIChE J.*, **40**, 1093 (1994).
43. Y. X. Guo, M. N. Rathor and H. C. Ti, *Chem. Eng. J.*, **67**, 205 (1997).
44. G. A. Hill and C. W. Robinson, *Biotechnol. Bioeng.*, **17**, 1599 (1975).
45. M. Schroeder, C. Muller, C. Posten, W. D. Deckwer, and V. Hecht, *Biotechnol. Bioeng.*, **54**, 567 (1997).